



NRC Publications Archive Archives des publications du CNRC

Ab initio structure determination of the low-temperature phase of succinonitrile from laboratory X-ray powder diffraction data - coping with potential poor powder quality using DFT ab initio methods

Whitfield, Pamela; Le Page, Yvon; Abouimrane, A.; Davidson, Isobel

This publication could be one of several versions: author's original, accepted manuscript or the publisher's version. / La version de cette publication peut être l'une des suivantes : la version prépublication de l'auteur, la version acceptée du manuscrit ou la version de l'éditeur.

For the publisher's version, please access the DOI link below. / Pour consulter la version de l'éditeur, utilisez le lien DOI ci-dessous.

Publisher's version / Version de l'éditeur:

<https://doi.org/10.1154/1.3009635>

Powder Diffraction, 23, December 4, pp. 292-299, 2008

NRC Publications Record / Notice d'Archives des publications de CNRC:

<https://nrc-publications.canada.ca/eng/view/object/?id=35373b0f-e6e6-44b0-9c7e-02be3425f14e>

<https://publications-cnrc.canada.ca/fra/voir/objet/?id=35373b0f-e6e6-44b0-9c7e-02be3425f14e>

Access and use of this website and the material on it are subject to the Terms and Conditions set forth at

<https://nrc-publications.canada.ca/eng/copyright>

READ THESE TERMS AND CONDITIONS CAREFULLY BEFORE USING THIS WEBSITE.

L'accès à ce site Web et l'utilisation de son contenu sont assujettis aux conditions présentées dans le site

<https://publications-cnrc.canada.ca/fra/droits>

LISEZ CES CONDITIONS ATTENTIVEMENT AVANT D'UTILISER CE SITE WEB.

Questions? Contact the NRC Publications Archive team at

PublicationsArchive-ArchivesPublications@nrc-cnrc.gc.ca. If you wish to email the authors directly, please see the first page of the publication for their contact information.

Vous avez des questions? Nous pouvons vous aider. Pour communiquer directement avec un auteur, consultez la première page de la revue dans laquelle son article a été publié afin de trouver ses coordonnées. Si vous n'arrivez pas à les repérer, communiquez avec nous à PublicationsArchive-ArchivesPublications@nrc-cnrc.gc.ca.



***Ab initio* structure determination of the low-temperature phase of succinonitrile from laboratory X-ray powder diffraction data—Coping with potential poor powder quality using DFT *ab initio* methods**

P. S. Whitfield, Y. Le Page, A. Abouimrane, and I. J. Davidson

Institute for Chemical Process and Environmental Technology, National Research Council Canada, 1200 Montreal Road, Ottawa, Ontario K1A 0R6, Canada

(Received 21 July 2008; accepted 10 September 2008)

Without experimental or predicted literature crystal structures for succinonitrile at low temperature, structure solution was attempted from powder diffraction data taken at 173 and 90 K from a solid sample. Its room-temperature plastic-crystal state makes production of a sample with good particle statistics and random orientation almost impossible. Combining constrained models, simulated annealing, and careful application of second-order spherical harmonic corrections nevertheless produced viable-looking structures at 90 and 173 K, yielding two distinct structure models with the same projection down *c*. VASP optimization of atom coordinates in the experimental cell agreed well with the 90 K model but poorly with the model derived from the 173 K data. The refined 90 K structure changed little on optimization and fitted all datasets from 85 to 225 K. Plots of cell data, torsion angles, and isotropic displacement parameters against temperature suggest possible phase transitions around 100, 120, and 180 K. Cell data at 90 K: monoclinic $P2_1/a$, $a=9.0851(5)$ Å, $b=8.5617(5)$ Å, $c=5.8343(3)$ Å, $\beta=79.295(2)^\circ$, and $Z=4$. Succinonitrile has *gauche* conformation, in agreement with literature spectroscopy data. © 2008 Crown of Canada. [DOI: 10.1154/1.3009635]

Key words: structure solution, DFT methods, simulated annealing, nonambient diffraction

I. INTRODUCTION

Succinonitrile is an interesting material because of the ability of its ambient-temperature plastic-crystal phase (Sherwood, 1979) to dissolve many inorganic salts, and under certain circumstances to form intricate self-assembling network coordination compounds (Carlucci *et al.*, 2002; Whitfield *et al.*, 2007a). The solvating properties of succinonitrile in the plastic-crystal state, with subsequent good ionic transport properties, have made it a potential base for solid electrolytes for lithium battery materials (Alarco *et al.*, 2004; Long *et al.*, 2003; Abouimrane *et al.*, 2007). Succinonitrile exhibits a transition from the room-temperature cubic plastic-crystal containing both *gauche* and *trans* conformers (Fengler and Ruoff, 2001) to an ordered crystalline phase on cooling below 230 K (Janz and Fitzgerald, 1955). There are a number of literature papers describing the rotational and conformational disorder in the plastic crystal phase (Derollez *et al.*, 1990), but little other than spectroscopy (Fengler and Ruoff, 2001; Janz and Fitzgerald, 1955) and thermal analysis data (Alarco *et al.*, 2004; Badea *et al.*, 2007) describing the low-temperature phase. Statements that it is monoclinic (Fengler and Ruoff, 2001; Badea *et al.*, 2007) with space group $P2_1/a$ (Badea *et al.*, 2007) appear, but we have found no definitive information to date as to how these data were derived. Spectroscopy data have shown that the molecules in the low-temperature form are solely in the *gauche* conformation (Janz and Fitzgerald, 1955). The number of molecules in the unit cell has also been assigned as $Z=4$ (Fengler and Ruoff, 2001). During a variable temperature phase study of a potential electrolyte system, we collected low-temperature diffraction data of pure succinonitrile, providing the opportunity to study the low-temperature crystal structure of succinonitrile.

Succinonitrile is a challenging material for powder diffraction analysis because of its plastic state and sticky nature at room temperature. Optimizing the particle statistics by producing a micron-sized powder may be possible using cryomilling. In all other situations the possibility of poor statistics is always present with subsequent errors in relative peak intensities (Smith, 2001). The low linear absorption coefficient of succinonitrile with Cu $K\alpha$ makes analysis in transmission preferable to reflection, but getting the sample inside the capillary is more difficult than for most materials. Melting the sample by heating to 60 °C and injecting the liquid into the capillary before cooling is the most practical approach, but this leads to a single lump of plastic crystal. An additional complication is that succinonitrile is a classical example of a system where dendritic and directional crystal growth can occur (Glicksman *et al.*, 1976; Fedorov *et al.*, 2005), which could lead to significant orientation issues inside a capillary. Although capillaries are usually a way of avoiding orientation with platelike morphologies, they can make the orientation of fiberlike materials worse. It is possible that the combination of orientation and poor statistics has hindered previous attempts to solve the crystal structure of the low-temperature form from powder diffraction. Any particle statistics problem could be addressed, at least partially, using a 2D detector, but the orientation issue would remain. Single crystal diffraction would normally solve such a small-molecule structure with ease, but again the plastic-crystal nature of the phase may also have hindered good-quality low-temperature data from being obtained.

We determine here the crystal structure of succinonitrile in two *ab initio* steps completed by a rigid-body refinement, based on its low-temperature powder diffraction data at

173 K and then at 90 K after recrystallizing the sample *in situ*. The first *ab initio* step was the derivation of a crude conformation, orientation, and position for the molecule with the help of recent structure-determination methods using minimal prior information and thus often called *ab initio* methods, as implemented in DIFFRACPlus TOPAS (Bruker-AXS). The second *ab initio* step was a DFT optimization with VASP (Kresse, 1993; Kresse and Hafner, 1993, 1994) of this crude conformation, orientation, and position of the molecule in its accurate experimentally determined cell. Inexpensive computers capable of performing DFT optimization of even large crystal-structure models have recently become available. The combination of powder methods and DFT methods is quite intuitive, and accordingly becoming more widespread. Depending on the desired amount of experimental content of the printed results, this combination can take several forms. At one end of the spectrum, Mercier *et al.* (2007) salvage as much experimental content as possible in a nevertheless numerically stable refinement by constraining a single chemically uninterpretable angle in a parametrized description of apatites to its DFT-calculated value. At the other end, Smrčok *et al.* (2007) advocate complete replacement of Rietveld refinement of organic molecular crystals by their DFT optimization. There are many intermediate possibilities for combinations (Dinnebier *et al.*, 2001; Neumann *et al.*, 2002; Baikie *et al.*, 2007; Whitfield *et al.*, 2007b). Here, the use of DFT methods helped us label as wrong an otherwise plausible rigid-body structure model from standard X-ray structure solution methods.

II. EXPERIMENTAL

The data were obtained from a Cu $K\alpha$ Bruker D8 Advance diffractometer. The diffractometer was equipped with a focusing primary mirror and a Vantec PSD detector with radial Soller slits. The mirror was effective in suppressing the $K\beta$ line, so a filter was not necessary. The temperature of the sample was controlled using a custom-built cryoflow system (Cryosystems of America, Inc.) with the nozzle geometry colinear with the capillary to reduce turbulence and consequent icing of the sample. A goniometer heat shield (Cryo Positioning Systems) was used to prevent the goniometer head from icing. A Lakeshore 331S cryocontroller was used to maintain a constant temperature. A 4 mm Debye slit was used in the detector so the detector only “saw” the sample in the constant temperature zone along the capillary. The temperature calibration of the cryoflow system was checked previously using the thermal expansion of aluminium powder and phase transitions of NH_4NO_3 and found to be reproducible.

For the 173 K dataset, the succinonitrile (99%, Aldrich) was melted and injected into a 0.5 mm borosilicate capillary before cooling to room temperature in ambient conditions. Another set of data was obtained after melting the sample in the capillary and cooling down to 85 K while rotating the sample. Data were then obtained between 85 and 355 K in 5 K steps. Data were taken with a 10° window between 5 and $80^\circ 2\theta$ using a 0.0214° step size and an effective 1 s count time.

All of the data analysis was performed using DIFFRAC-Plus TOPAS (Bruker-AXS) on raw, unprocessed data. Crys-

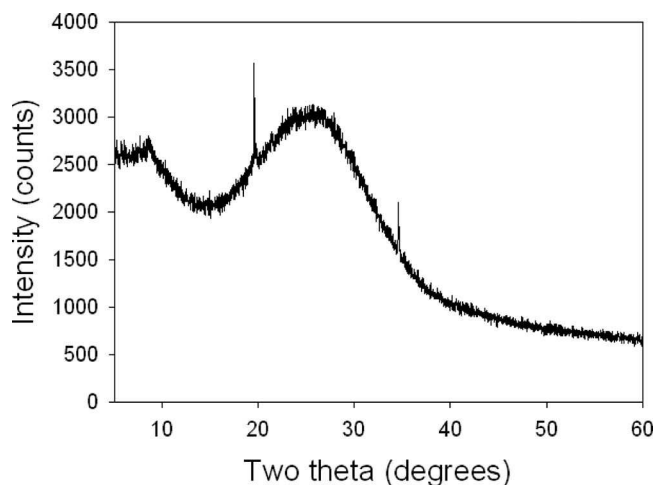


Figure 1. Room-temperature diffraction pattern of the succinonitrile before cooling to 173 K. The weak reflections correspond to the poorly crystalline cubic $Im\bar{3}m$ plastic-crystal phase.

tallite size-constrained single peak fitting produced the input data for indexing using the singular value decomposition method (Coelho, 2003). All possible symmetries from cubic to primitive monoclinic were examined. The ratio of possible unobserved to observed reflections was set as 12. The highest ranked solution with no unindexed lines was a cell in $P2_1$ with a GOF of 34.6. Automated Pawley fitting (Pawley, 1981) of the candidate unit cells with the GOFs down to 20 was used to confirm the quality of the fit of the cells to the experimental data before proceeding further. The TOPAS indexing software produces a suggested space group, but an analysis using Extsym (Markvardsen *et al.*, 2001) was also used to examine the possible space groups in terms of maximum likelihood. Extsym examines the systematic absences in a Pawley fit of the lowest applicable symmetry, in this case $P2_1$, to rank the most likely extinction symbols.

A. *Ab initio* structure solution

The diffraction pattern of the succinonitrile at room temperature before cooling is shown in Figure 1. Although

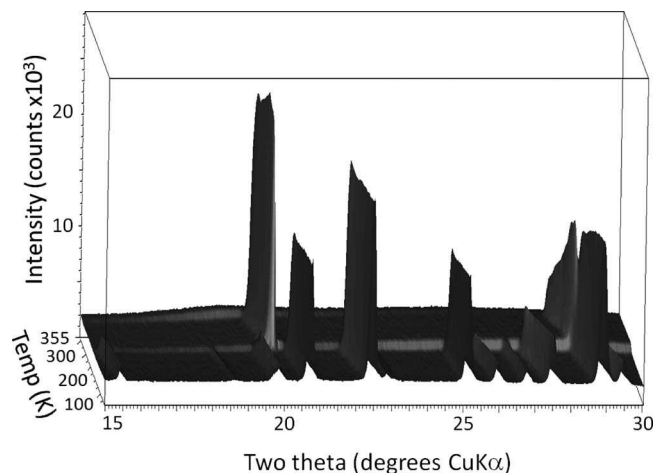


Figure 2. Powder diffraction data from succinonitrile between 85 and 355 K.

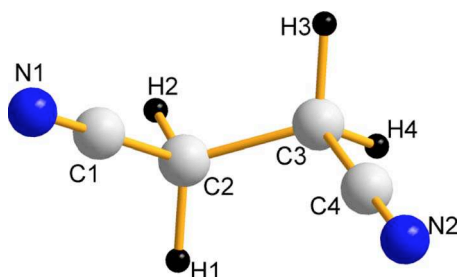


Figure 3. (Color online) Rigid-body succinonitrile molecule produced from the optimized 90 K structure.

mostly amorphous, reflections corresponding to the cubic $Im\bar{3}m$ plastic-crystal unit cell can be seen. The full range of experimental data can be seen in Figure 2, showing the low-temperature crystalline to plastic-crystal transition at 230 K, and the melting at 330 K.

Given the likely orientation bias in the experimental data, the use of z -matrix rigid-body constrained simulated annealing (SA) was preferable to charge-flipping (Oszlányi and Sütö, 2004). The z -matrix was constructed such that the conformation of the succinonitrile was randomly assigned to *cis*, *trans*, or *gauche* before each cycle. Forcing the molecule to restart in one of the possible conformations as opposed to a freely refined torsion angle once again acted as a constraint against bias from orientation and possibly unreliable relative intensities. Bond lengths, bond angles, and torsion angles were constrained to chemically reasonable values (Lide, 2007) for the solution step.

One approach to account for preferential orientation during the SA of the 173 K dataset was adding a March-Dollase parameter (Dollase, 1986). Given the cubic nature of the plastic-crystal succinonitrile and lack of any obvious direction, an assumption had to be made regarding the orientation direction. The March-Dollase correction along the assumed $[100]$ direction had a variable constrained between the values of 0.8 and 1.2 in order to maintain stability during the SA. However, visual comparison with a structure proposed from parallel work by a group using synchrotron data (Hore *et al.*, 2008) indicated that the assumed direction biased the SA to the point where the correct minimum had not been found. In the event, it would appear as though the March-Dollase approach with the $[100]$ direction would have been perfectly adequate for the 90 K dataset, but the 173 K dataset was attempted first. The spherical harmonics approach (Von Dreele, 1997) has the advantage of no assumed orientation

TABLE I. Bond lengths from the 90 K DFT-optimized structure.

Atom pair	Optimized bond length (Å)
N1-C1	1.1633
C1-C2	1.4504
C2-C3	1.5396
C3-C4	1.4511
C4-N2	1.1645
C2-H1	1.0989
C2-H2	1.0975
C3-H3	1.0998
C3-H4	1.0960

TABLE II. Selected bond angles from the 90 K DFT-optimized structure.

Atom group	Bond angle (°)	Torsion angle (°)
C4-C3-C2	112.997	—
N2-C4-C3	179.330	—
C1-C2-C3	112.964	—
N1-C1-C2	178.488	—
C1-C2-C3-C4	—	60.396

direction but would normally be too likely to destabilize an SA run. In an attempt to stabilize the coefficients, a second-order correction was added (three variables in this case) using the TOPAS macro language command “val_on_continue” to force the values to reset to zero after each minimization cycle. The TOPAS “decomposition” option was used for the

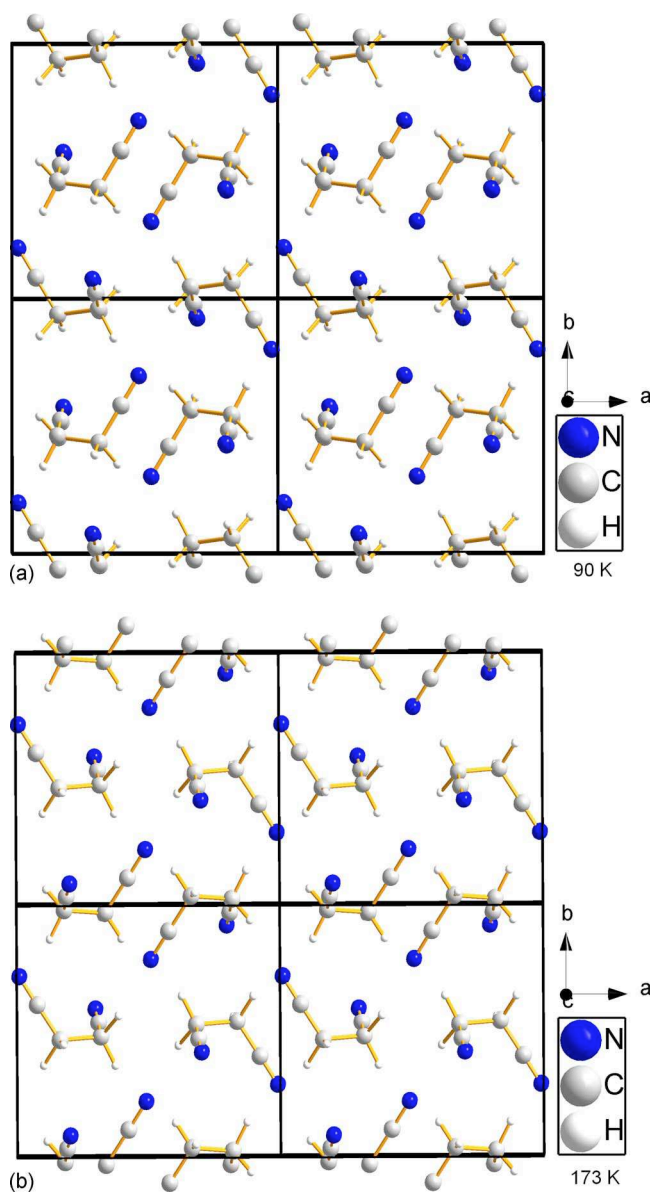


Figure 4. (Color online) Projections down the c axis for the optimized structures from the (a) 90 K solution and (b) 173 K solution. The structures are not related by any symmetry operation, although visually from the view along the c axis, it might be expected that they are related by an origin shift.

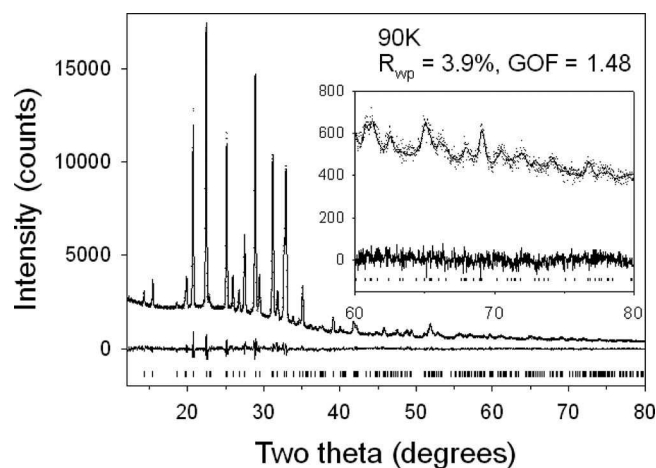


Figure 5. Rietveld difference plot of the 90 K DFT *ab initio* derived rigid body to the 90 K experimental data. The high-angle portion of the difference plot is magnified in the inset.

simulated annealing where the peak intensities are used alone in order to speed up the calculation. Datasets taken at both 90 and 173 K were used in SA runs. For the refinement step, a fourth-order spherical harmonics correction was used.

B. DFT *ab initio* structure optimization

The conformation of the models obtained from X-ray refinement were clear but had very crude distances and angles. We accordingly optimized the atom coordinates of the structures obtained from the 90 and 173 K data with DFT (density functional theory) methods, while retaining their experimental unit cell dimensions. Optimization was performed with VASP using input files prepared, and output files interpreted with the *Materials Toolkit* (Le Page and Rodgers, 2005) environment for *ab initio* modeling of materials. The GGA PAW potentials (Kresse and Joubert, 1999) for C, N, and H atoms were used for all calculations with 400 eV energy cutoff. Wave functions were optimized iteratively with the Davidson blocked scheme in combination with reciprocal space projectors (Davidson, 1983) down to an electronic convergence of 1×10^{-7} eV. A Monkhorst-Pack scheme (Monkhorst and Pack, 1976) was used to perform reciprocal space integration. Energy corrections were applied according to the Methfessel-Paxton smearing scheme with order 1 and width 0.2 eV (Methfessel and Paxton, 1989). The convergence criterion for forces was 1×10^{-4} eV/Å. No spin polarization corrections were performed. A $3 \times 3 \times 3$ k mesh was used for all calculations, ensuring a reciprocal resolution better than 0.07 Å^{-1} in all directions.

Convergence of the 173 K model was slow but steady, with no drastic change to the model, apart from a regularization of distances and angles. The slow convergence speed was a result of “ringing” of the molecule each time an atom-position adjustment altered a bond length, but the total energy went down steadily without quite reaching the minimum total energy of the 90 K model. The initial total energy of the 90 K X-ray model was 9 eV lower than the initial total energy of the 173 K model and converged rapidly with next to no change. This indicated excellent agreement between

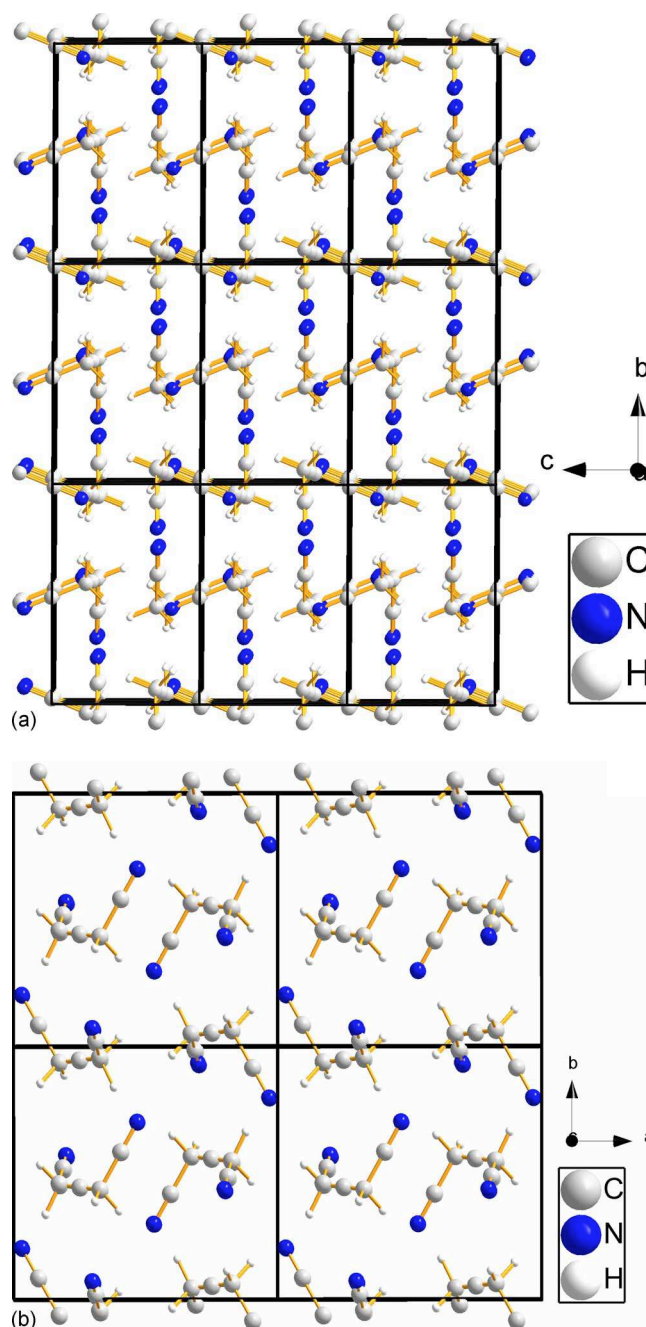


Figure 6. (Color online) Projections of the succinonitrile structure at 90 K down (a) the *a* direction and (b) *c* direction.

the X-ray model and its DFT optimization for the 90 K model, but poor agreement for the 173 K model.

C. Rigid-body X-ray re-optimization based on DFT *ab initio* geometry

A rigid-body *z*-matrix was constructed from the 90 K optimized succinonitrile molecule (Figure 3) for refinement of the molecular arrangement against the experimental data. Bond lengths, bond angles, and torsion angles were extracted from the optimized succinonitrile molecule as shown in Tables I and II. The refined variables were limited to the translation and rotation of the rigid-body, lattice parameters, zero point error, background, separate B_{iso} for N and (C,H),

TABLE III. Atomic coordinates for the 90 K DFT-optimized succinonitrile molecule refined against the experimental data at 90 K.

Atom	<i>x</i>	<i>y</i>	<i>z</i>
C1	0.3119(2)	0.0175(3)	0.0069(5)
C2	0.3262(3)	0.9540(4)	0.7733(5)
C3	0.1732(4)	0.9359(4)	0.6988(3)
C4	0.0948(3)	0.0838(4)	0.7021(2)
N1	0.3005(4)	0.0684(5)	0.1942(5)
N2	0.0320(4)	0.2025(4)	0.7047(5)
H1	0.3996(3)	0.0329(5)	0.6550(5)
H2	0.3798(5)	0.8387(4)	0.7645(7)
H3	0.1023(5)	0.8528(4)	0.8137(6)
H4	0.1914(5)	0.8877(5)	0.5218(4)

$a=9.0851(5)$ Å, $b=8.5617(5)$ Å, $c=5.8343(3)$ Å, $\beta=79.295(2)^\circ$; space group $P2_1/a$, $B_{\text{iso}}(\text{C,H})=3.1(1)\text{\AA}^2$, $B_{\text{iso}}(\text{N})=3.4(1)\text{\AA}^2$, C2-C3 torsion angle $=59.34(3)^\circ$; $R_{\text{wp}}=3.88$, GOF=1.46, DW=1.65.

and a fourth-order spherical harmonics preferential orientation correction. The terminal C-C-C bond angles were also refined but constrained to have equal values to reduce correlations. The very close values for these angles in the optimized structure would appear to make this a reasonable assumption. The cycle of optimization and refinement was repeated twice. The final refinement errors were calculated using the bootstrap method (Efron and Tibshirani, 1986), as the errors in fractional coordinates in a z -matrix cannot be determined in TOPAS using matrix inversion. This method carries out a series of refinements (in this case 100) with a portion of the observed intensities modified, with the standard deviation of the refined values becoming the bootstrap errors (see the DIFFRACplus TOPAS: TOPAS 4 user manual).

III. RESULTS AND DISCUSSION

A. Comparison with literature results

The maximum likelihood results from Extsym (Markvardsen *et al.*, 2001) suggested that the most likely extinction symbols in order of probability were $P1a1$ (15.3), $P12_1/a1$ (10.8), and $P12_11$ (3.4). The extinction symbol $P1a1$ contains the space group $P2/a$ in addition to Pa (Looijenga-Vos

and Buerger, 2006). The solution in $P2/a$ was extremely poor, yielding an R_{wp} value of 35.6. $P2_1/a$ agrees with the sole literature assignment (Badea *et al.*, 2007), but solutions were attempted in all these space groups. Actually, the solution in space group Pa , which is a subgroup of both space groups $P2/a$ and $P2_1/a$, produced candidate structures that were very similar to those for space group $P2_1/a$. Initial refinement using space group Pa produced a slightly better fit than $P2_1/a$ (R_{wp} of 6.4% and 7.0%, respectively), but that is expected given the extra degrees of freedom in a subgroup. A number of the bond and torsion angles in the Pa structure went well beyond reasonable values, while the single z -matrix in the $P2_1/a$ cell refined to reasonable values even if some of the bond lengths were rather long. It is quite possible that the Pa structure had more degrees of freedom than the data could support. Pawley fits of the experimental data to the unit cell in Pa and $P2_1/a$ yielded identical fits, and indeed optimization of the Pa structure produced a structure indistinguishable to the $P2_1/a$ solution. The solution was pursued in $P2_1/a$ as opposed to the transformed $P2_1/c$ cell to facilitate comparison with other studies.

B. The two solutions and their discrimination

The SA found satisfactory-looking solutions for both the 173 and 90 K datasets, with raw, unrefined R_{wp} values of 8.5% and 7.0%, respectively. The SA solutions from the datasets at 173 and 90 K were found to be different, although looking at the projections in the c direction (Figure 4) it seems as though they should be related by an origin shift, but they are not. The initial refined structure from the 90 K data was found to be 9 eV lower in energy than the refined 173 K structure because the 173 K structure had drifted away from chemically reasonable bond lengths during X-ray optimization. This is not an issue with the temperature, but with the model, as a separate solution using the 175 K dataset from the recrystallized sample produced a solution identical to the 90 K solution.

The fits obtained after Rietveld refinement are good as seen in Figure 5, with an R_{wp} residual for the 90 K refinement of 3.9%, a GOF of 1.48, and a Durban-Watson statistic of 1.5. The packing of the structure at 90 K along the a and c axes can be seen in Figure 6. The projection along the c axis appears identical to that in Hore *et al.* (2008), but without cell data and atomic coordinates, it was not possible to directly compare the two. It must be noted that the false minima found with the 173 K data also looked the same along the c direction. However, it was not energetically stable and produced a significantly different calculated powder pattern after DFT optimization.

C. Possible phase transitions

The atomic coordinates of the 90 K optimized structure refined against the 90 and 225 K experimental data are given in Tables III and IV, respectively. Some of the structural parameters refined from the recrystallized sample between 85 and 225 K showed some interesting trends. Figure 7 shows the refined unit cell parameters and Figure 8 shows the B_{iso} values and central C-C torsion angles. The excursion in both $B_{\text{iso}}(\text{N})$ and $B_{\text{iso}}(\text{C,H})$ below 100 K suggests some kind of phase transition and is matched by what could be

TABLE IV. Atomic coordinates for the 90 K DFT-optimized succinonitrile molecule refined against the experimental data at 225 K.

Atom	<i>x</i>	<i>y</i>	<i>z</i>
C1	0.312 55(2)	0.020 64(5)	0.000 97(12)
C2	0.327 21(6)	0.956 10(4)	0.772 05(13)
C3	0.176 81(8)	0.938 16(5)	0.692 65(6)
C4	0.095 97(6)	0.082 79(7)	0.700 21(5)
N1	0.300 80(8)	0.072 40(7)	0.184 58(12)
N2	0.031 09(6)	0.198 86(9)	0.706 27(10)
H1	0.400 96(6)	0.032 85(8)	0.655 95(14)
H2	0.379 69(10)	0.841 88(6)	0.767 79(19)
H3	0.107 96(9)	0.852 37(7)	0.799 50(7)
H4	0.196 51(12)	0.894 83(6)	0.516 00(6)

$a=9.16156(2)$ Å, $b=8.65418(5)$ Å, $c=5.92118(1)$ Å, $\beta=79.9106(4)^\circ$; space group $P2_1/a$, $B_{\text{iso}}(\text{C,H})=5.77(3)\text{\AA}^2$, $B_{\text{iso}}(\text{N})=5.96(2)\text{\AA}^2$, C2-C3 torsion angle $=56.518(8)^\circ$; $R_{\text{wp}}=3.94$, GOF=1.40, DW=1.69.

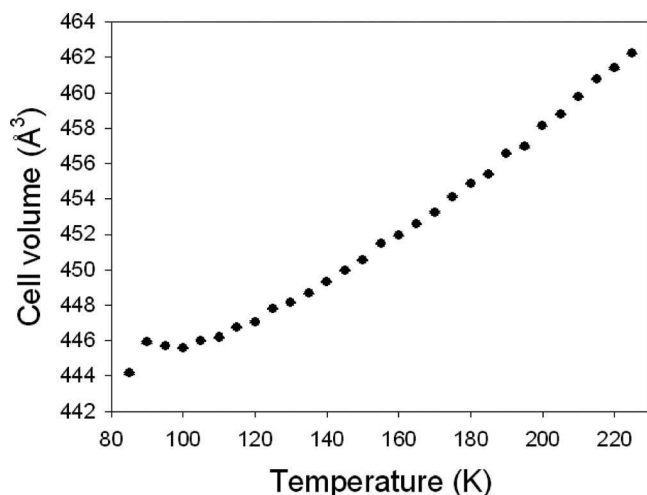


Figure 7. Refined unit cell volume for succinonitrile between 85 and 225 K.

negative thermal expansion between 90 and 100 K. The graph in Figure 9 showing the closest refined N-N contacts appears to indicate a definite transition below 120 K. The plateau in intermolecular N-N closest contact at about 3.58 Å corresponds very well with the step in plateau from $\sim 57.7^\circ$ to $\sim 59^\circ$ in torsion angles below 125 K seen in Figure 8. An additional change is visible in the torsion angles above 180 K, with a change from the plateau at $\sim 57.7^\circ$ to a sloping temperature dependence down to a torsion angle of 56.5° at 225 K.

The transition below 120 and 125 K appears to be related to intermolecular electrostatic effects given the behavior of the closest N-N contacts in Figure 9. The cause of the discontinuities in displacement parameters and lattice parameters below 110 K and the change in temperature dependence of the torsion angle above 180 K are as yet unexplained. The relatively poor counting statistics in the data above $40^\circ 2\theta$ in Figure 5 are very obvious. In order to extract additional structural subtleties, the counting statistics in the lower d -spacing range would have to be improved, possibly using a variable-count (Madsen and Hill, 1994) or pseudo-variable count time strategy in the data collection.

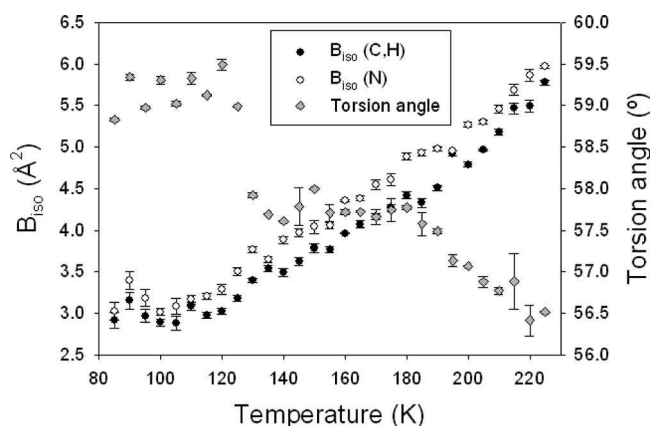


Figure 8. Plot of refined B_{iso} values and torsion angle versus temperature.

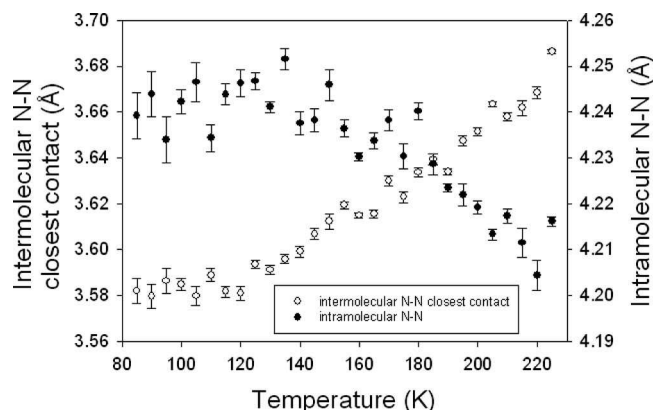


Figure 9. Variation in intra- and closest N-N intermolecular contact distances with temperature.

D. Texture analysis with spherical harmonics

The 90 K derived structure fitted the data from the recrystallized samples better than the structure derived from the original 173 K sample cooled in ambient air. Analysis of the spherical harmonics coefficients showed the texture index of the 173 K data refinement with the 90 K model to be 1.21 versus 1.06 for the refinement of the same structure against the 90 K data. This shows that recrystallizing the sample *in situ* by quenching/rapid cooling reduced significantly the orientation in this particular case.

Spherical harmonics orientation corrections can often improve the fit of Rietveld refinements, even where the data, structures, or both are questionable. Ideally, if the proposed structure is correct, the orientation should have a physical basis, e.g., probable direction of the crystallization front. GSAS (Larson and Von Dreele, 1994) was used to plot the axial distributions from the spherical harmonics coefficients. Capillary geometry simplifies the texture significantly. The gamma angle becomes meaningless and the psi angle is simply the angle away from the central axis of the capillary.

The coefficients for the refinements of the 173 K and recrystallized 90 K data are significantly different, and the analysis reinforced this fact as shown in the axial distributions in Figures 10 and 11. The data for the recrystallized

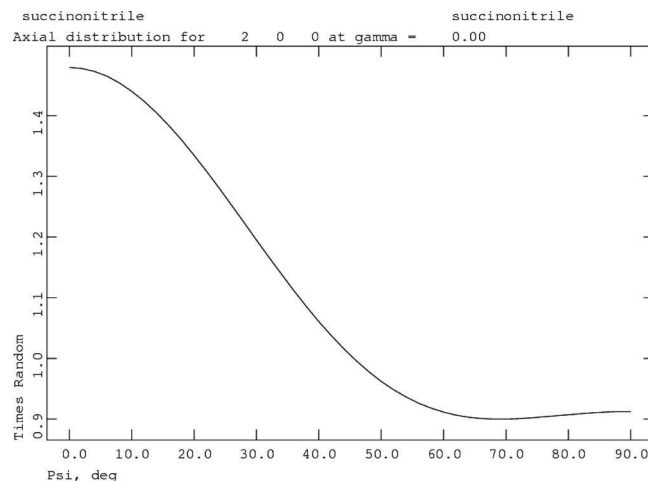


Figure 10. Axial distribution calculated along 200 using the refined fourth-order spherical harmonics coefficients for the 90 K dataset.

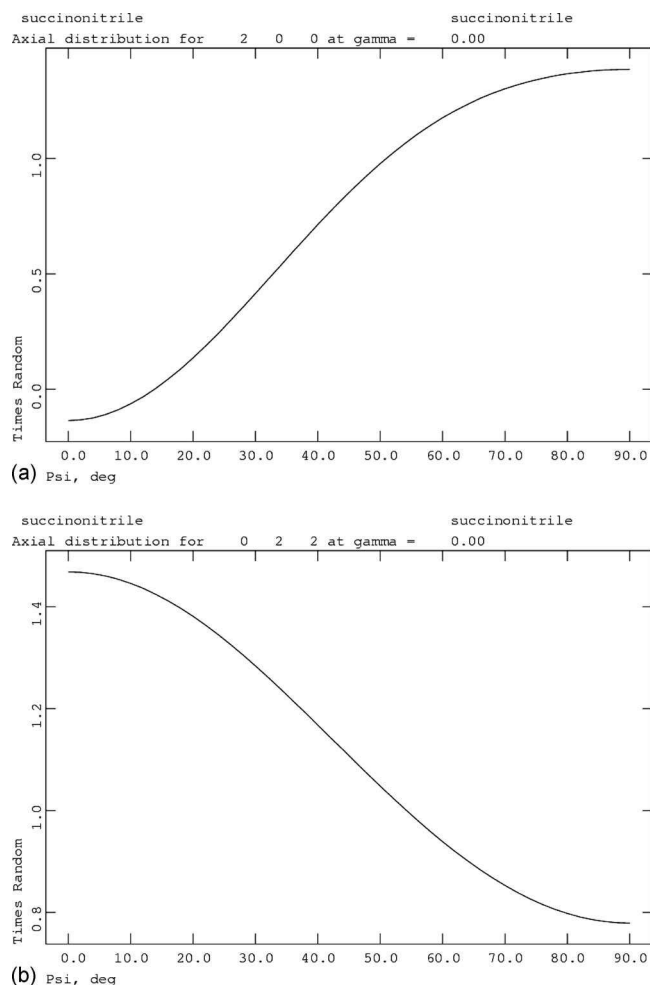


Figure 11. Axial distribution calculated along (a) 200 and (b) 022 using the refined fourth-order spherical harmonics coefficients for the 173 K dataset.

sample at 90 K show the cylinder axis to be oriented along the [100] direction, whereas Figure 11(a) shows that the [100] direction is perpendicular to the cylinder axis in the 173 K dataset. Figure 11(b) shows that for the 173 K dataset, it is the [022] direction that is orientated along the cylindrical axis. This helps explain why the constrained March-Dollase correction with [100] direction was ineffective in the solution step with the 173 K data, but it would have been perfectly adequate with the 90 K data.

The well-documented crystallization behavior of plastic-crystal succinonitrile in the presence of temperature gradients (Fedorov *et al.*, 2005) may provide a clue as to the origin of the drastically different texture of the two datasets. While the 173 K sample was cooled in ambient lab conditions before further cooling, the 90 K sample was crystallized *in situ* directly from the melt using the cryoflow apparatus. With ambient air and slow cooling the dominant temperature gradient is likely to be across the capillary, whereas rapid cooling with the cryoflow system will tend to produce a gradient mostly parallel to the nozzle along the capillary axis. This suggests that the succinonitrile tended to crystallize along the [100] direction following the temperature gradient during the transition from the plastic-crystal phase. How much this crystallization behavior depends on the plastic-crystal orientation is uncertain, but in many ways

the plastic-crystal phase behaves very much like a fluid with regard to transport properties (Alarco *et al.*, 2004) because of the orientational disorder, so it is possible that it may also impact the low-temperature crystallization process.

IV. CONCLUSION

A combination of simulated annealing and *ab initio* DFT optimization has been used to obtain a rigid-body structure for succinonitrile at low temperature. The use of continually resetting second-order spherical harmonics was found to be more reliable than a constrained March-Dollase correction because of the lack of an assumed *hkl* direction. Two solutions were obtained, one at 90 K and the other at 173 K. The structure obtained from the 90 K data has been demonstrated to be the correct one by DFT optimization. The unit cell was found to be monoclinic in $P2_1/a$ with $Z=4$, and the succinonitrile molecules are in the *gauche* conformation in agreement with literature spectroscopy data. The optimized structure was used to refine structural changes in a series of datasets taken between 85 K and just below the plastic-crystal transition at 225 K.

It is worth noting that the solution of the 173 K X-ray data set produced by simulated annealing yielded a model that may have sounded quite plausible in the absence of the correct 90 K solution in view of the X-ray residuals, quality factors, and possibly questionable relative intensities. Even in the absence of a competing model, DFT *ab initio* optimization methods could label the 173 K model as dubious and probably from a false minimum: the model drifted so far away from its X-ray assigned position and orientation that the powder pattern recalculated from DFT-optimized coordinates had little similarity with the experimental one. In contrast, in the absence of a competing model, the 90 K model could be labeled as most certainly the correct global minimum from simulated annealing, as it did not change significantly under DFT optimization. This observation underscores the usefulness of DFT software as a complement for structure solution from powder diffraction data using global optimization techniques, such as simulated annealing. The uncertainty in such techniques as to whether the real global minimum has been found is always a concern, especially where the use of constraints and penalty functions can bias the result.

The “correct” solution produces low X-ray data residuals, a chemically plausible model within experimental error, and resides at an *ab initio* total-energy minimum. This again demonstrates the complementarity of experimental diffraction and DFT *ab initio* methods in structural investigations.

Although the transition below 120 to 125 K may be a result of intermolecular electrostatic interactions between the nitrogens, the apparent transitions below 110 K and above 180 K currently cannot be explained using the structural models used in the analysis. Explanations may become apparent with higher quality data with improved counting statistics to lower *d*-spacings, to allow independent refinement of all the structural parameters.

ACKNOWLEDGMENTS

The authors thank Robert Von Dreele of Argonne National Laboratory for suggestions regarding the texture

analysis and Robert Dinnebier of the Max-Planck Institute for Solid State Research for discussions about their results on the structure of succinonitrile and a preprint of his paper prior to submission. The work was partly funded by the Canadian Government Technology and Innovation Initiative and the Canadian Department of National Defense.

Abouimrane, A., Whitfield, P. S., Niketic, S., and Davidson, I. J. (2007). "Investigation of Li salt doped succinonitrile as potential solid electrolytes for lithium batteries," *J. Power Sources* **174**, 883–888.

Alarco, P.-J., Abu-Lebdeh, Y., Abouimrane, A., and Armand, M. (2004). "The plastic-crystalline phase of succinonitrile as a universal matrix for solid-state ionic conductors," *Nature Mater.* **3**, 476–481.

Badea, E., Blanco, I., and Gatta, G. D. (2007). "Fusion and solid-to-solid transitions of a homologous series of alkane- α , ω -dinitriles," *J. Chem. Thermodyn.* **39**, 1392–1398.

Baikie, T., Mercier, P. H. J., Elcombe, M. M., Kim, J. Y., Le Page, Y., Mitchell, L. D., White, T. J., and Whitfield, P. S. (2007). "Triclinic apatites," *Acta Crystallogr., Sect. B: Struct. Sci.* **63**, 251–256.

Carlucci, L., Ciani, G., Proserpio, D. M., and Rizzato, S. (2002). "Coordination networks from the self-assembly of silver salts and the linear chain dinitriles NC(CH₂)_nCN ($n=2$ to 7): A systematic investigation of the role of counterions and of the increasing length of the spacers," *Crystr. Eng. Commun.* **4**, 413–425.

Coelho, A. A. (2003). "Indexing of powder diffraction patterns by iterative use of singular value decomposition," *J. Appl. Crystallogr.* **36**, 86–95.

Davidson, E. R. (1983). "Matrix eigenvector methods," in *Methods in Computational Molecular Physics*, edited by G. H. F. Diercksen and S. Wilson (Plenum, New York), pp. 95–113.

Derollez, P., Lefebvre, J., Descamps, M., Press, W., and Fontaine, H. (1990). "Structure of succinonitrile in its plastic phase," *J. Phys.: Condens. Matter* **2**, 6893–6903.

Dinnebier, R. E., Ding, L., Ma, K., Neumann, M. A., Tanpipat, N., Leusen, F. J. J., Stephens, P. W., and Wagner, M. (2001). "Crystal structure of a rigid ferrocene-based macrocycle from high-resolution X-ray powder diffraction," *Organometallics* **20**, 5642–5647.

Dollase, W. A. (1986). "Correction of intensities for preferred orientation in powder diffractometry: Application of the March model," *J. Appl. Crystallogr.* **19**, 267–272.

Efron, B. and Tibshirani, (1986). "Bootstrap methods for standard errors, confidence intervals, and other measures of statistical accuracy," *Stat. Sci.* **1**, 54–77.

Fedorov, O. P., Shpak, A. P., Zhivolub, E. L., and Shuleshova, O. V. (2005). "The influence of crystalline anisotropy on the evolution of the crystallization front during directional solidification," *Crystallogr. Rep.* **50**, 1027–1033.

Fengler, O. I. and Ruoff, A. (2001). "Vibrational spectra of succinonitrile and its [1,4-¹³C₂]-, [2,2,3,3-²H₄]- and [1,4-¹³C₂-2,2,3,3-²H₄]-isotopomers and a force field of succinonitrile," *Spectrochim. Acta, Part A* **57**, 105–117.

Glicksman, M. E., Scafer, R. J., and Ayers, J. D. (1976). "Dendritic growth—a test of theory," *Metall. Trans. A* **7A**, 1747–1759.

Hore, S., Dinnebier, R., Wen, W., Hanson, J., Belabbas, I., Carlsson, J. M., Scheffler, M., and Maier, J. (2008). "High resolution *in situ* powder diffraction of highly disordered plastic crystal, namely succinonitrile," *Z. Anorg. Allg. Chem.* (in press).

Janz, G. J. and Fitzgerald, W. E. (1955). "Infrared spectrum and molecular structure of succinonitrile," *J. Chem. Phys.* **23**, 1973–1974.

Kresse, G. (1993). *Ab initio Molekular Dynamik für flüssige Metalle*, Ph.D. Thesis, Technische Universität Wien, Vienna, Austria.

Kresse, G. and Hafner, J. (1993). "Ab initio molecular dynamics for open-

shell transition metals," *Phys. Rev. B: Condens. Matter* **48**, 13115–13118.

Kresse, G. and Hafner, J. (1994). "Ab initio molecular-dynamics simulation of the liquid-metal-amorphous-semiconductor transition in germanium," *Phys. Rev. B: Condens. Matter* **49**, 14251–14269.

Kresse, G. and Joubert, D. (1999). "From ultrasoft pseudopotentials to the projector augmented-wave method," *Phys. Rev. B: Condens. Matter* **59**, 1758–1775.

Larson, A. C. and Von Dreele, R. B. (1994). *General Structure Analysis System (GSAS)* (Report LAUR 86–748). Los Alamos National Laboratory, Los Alamos, New Mexico.

Le Page, Y. and Rodgers, J. R. (2005). "Quantum software interfaced with crystal-structure databases: Tools, results and perspectives," *J. Appl. Crystallogr.* **38**, 697–705.

Lide, D. R. (Ed.) (2007). *CRC Handbook of Chemistry and Physics*, 88th ed. (CRC, Cleveland).

Long, S., MacFarlane, D. R., and Forsyth, M. (2003). "Fast ion conduction in molecular plastic crystals," *Solid State Ionics* **161**, 105–112.

Looijenga-Vos, A. and Buerger, M. J. (2006). "Space-group determination and diffraction symbols," in *International Tables for Crystallography*, edited by Th. Hahn (IUCr, Chester), Vol. A, pp. 44–54.

Madsen, I. C. and Hill, R. J. (1994). "Collection and analysis of powder diffraction data with near-constant counting statistics," *J. Appl. Crystallogr.* **27**, 385–392.

Markvardsen, A. J., David, W. I. F., Johnston, J. C., and Shankland, K. (2001). "A probabilistic approach to space-group determination from powder diffraction data," *Acta Crystallogr., Sect. A: Found. Crystallogr.* **57**, 47–54.

Mercier, P. H. J., Dong, Z., Baikie, T., Le Page, Y., White, T. J., Whitfield, P. S., and Mitchell, L. D. (2007). "Ab initio constrained crystal-chemical Rietveld refinement of Ca₁₀(V_xP_{1-x}O₄)F₂ apatites," *Acta Crystallogr., Sect. B: Struct. Sci.* **63**, 37–48.

Methfessel, M. and Paxton, A. T. (1989). "High-precision sampling for Brillouin-zone integration in metals," *Phys. Rev. B: Condens. Matter* **40**, 3616–3621.

Monkhorst, H. J. and Pack, J. D. (1976). "Special points for Brillouin-zone integrations," *Phys. Rev. B: Condens. Matter* **13**, 5188–5192.

Neumann, M. A., Tedesco, C., Destri, S., Ferro, D. R., and Porzio, W. (2002). "Bridging the gap—structure determination of the red polymorph of tetrahexylsextithiophene by Monte Carlo simulated annealing, first-principles DFT calculations and Rietveld refinement," *J. Appl. Crystallogr.* **35**, 296–303.

Oszlányi, G. and Sütö, A. (2004). "Ab initio structure solution by charge flipping," *Acta Crystallogr., Sect. A: Found. Crystallogr.* **60**, 134–141.

Pawley, G. S. (1981). "Unit-cell refinement from powder diffraction scans," *J. Appl. Crystallogr.* **14**, 357–361.

Sherwood, J. N. (1979). *The Plastically Crystalline State* (Wiley, London).

Smith, D. K. (2001). "Particle statistics and whole-pattern methods in quantitative X-ray powder diffraction analysis," *Powder Diffr.* **16**, 186–191.

Smrčok, Ľ., Jorík, V., Scholtzová, E., and Milata, V. (2007). "Ab initio structure determination of 5-anilino-methylene-2,2-dimethyl-1,3-dioxane-4,6-dione from laboratory powder data—a combined use of X-ray, molecular and solid-state DFT study," *Acta Crystallogr., Sect. B: Struct. Sci.* **63**, 477–484.

Von Dreele, R. B. (1997). "Quantitative texture analysis by Rietveld refinement," *J. Appl. Crystallogr.* **30**, 517–525.

Whitfield, P. S., Abouimrane, A., and Davidson, I. J. (2007a). "Structure determination from powder diffraction data of some moisture-sensitive network coordination compounds," *Adv. X-Ray Anal.* **50**, 139–144.

Whitfield, P. S., Le Page, Y., Grice, J. D., Stanley, C. J., Jones, G. C., Rumsey, M. S., Blake, C., Roberts, A. C., Stirling, J. A. R., and Carpenter, G. J. C. (2007b). "LiNaSiB₃O₇(OH)—novel structure of the new borosilicate mineral jadarite determined from laboratory powder diffraction data," *Acta Crystallogr., Sect. B: Struct. Sci.* **63**, 396–401.